Calcium-Looping performance of steel and blast furnace slags for Thermochemical Energy Storage in Concentrated Solar Power plants

Jose Manuel Valverde [a*], Juan Miranda-Pizarro[a,c], Antonio Perejón[b,c],

Pedro E. Sánchez-Jiménez[c], Luis A. Pérez-Maqueda[c]

[a]Facultad de Fisica, Universidad de Sevilla, Avenida Reina Mercedes s/n, 41012 Sevilla, Spain.

[b]Departamento de Química Inorgánica, Facultad de Química, Universidad de Sevilla, C. Prof. García González 1, Sevilla 41071, Spain.

[c]Instituto de Ciencia de Materiales de Sevilla (C.S.I.C. - Universidad de Sevilla). C. Américo Vespucio 49, Sevilla 41092, Spain.

Abstract

The Calcium Looping (CaL) process, based on the carbonation/calcination of CaO, has been proposed as a feasible technology for Thermochemical Energy Storage (TCES) in Concentrated Solar Power (CSP) plants. The CaL process usually employs limestone as CaO precursor for its very low cost, non-toxicity, abundance and wide geographical distribution. However, the multicycle activity of limestone derived CaO under relevant CaL conditions for TCES in CSP plants can be severely limited by pore plugging. In this work, the alternative use of calcium-rich steel and blast furnace slags after treatment with acetic acid is investigated. A main observation is that the calcination temperature to regenerate the CaO is significantly reduced as compared to limestone. Furthermore, the multicycle activity of some of the slags tested at relevant CaL conditions for TCES remains high and stable if the treated samples are subjected to filtration. This process serves to remove silica grains, which helps decrease the porosity of the CaO resulting from calcination thus mitigating pore plugging.

Keywords: Steel slag, Blast furnace slag, Thermochemical Energy Storage, Calcium Looping, Concentrated Solar Power.

Corresponding Author

* E mail: jmillan@us.es

1. Introduction

The massive deployment of renewable energy technologies is an urgent need to limit global warming to 2 ºC over pre-industrial values in 2100 as was agreed in the 21st Climate Change Conference COP21 [1]. A critical challenge is to find efficient, low cost and environmentally friendly energy storage technologies to manage the intermittency of solar and wind as main renewable energy sources. Concentrated Solar Power (CSP) is a rapidly growing technology wherein the implementation of large scale energy storage at relatively low cost would be feasible [2]. A relevant advantage of CSP is that energy can be massively stored in a primary form such as high-temperature heat usable for generating electricity on demand. The present paper deals with energy storage in CSP plants with central tower technology in which a number of heliostats are distributed on the ground to reflect direct solar radiation into a receptor placed at the top of a tower where temperatures up to about 1000ºC can be achieved.

In currently commercial CSP plants with energy storage, heat is transferred in the solar receptor to a fluid composed of a mixture of nitrate salts, usually sodium nitrate ($NaNO_3$) and potassium nitrate (KNO_3) in a 60/40 percent ratio (solar salt) of high heat capacity. The solar salt is then transported into a hot salts tank where heat is stored as sensible heat (the energy density of solar salt is ~ 0.8 GJ/m^3) [3]. Storage of heat using molten solar salts allows for about 15 hours of autonomy in the absence of direct solar radiation [4]. However, the use of molten salts is hampered by their thermal decomposition at temperatures close to 600ºC [5]. Another inconvenient of molten salts is their relatively high freezing point, between 120-220ºC, which besides being a technological risk leads to relevant heat losses at night in deserted regions or high altitude areas where CSP technology allocation is more appropriate due to the elevated number of sun hours. A further drawback of solar salts is the impossibility of circulating them through standard conduction systems and valves because of their corrosiveness, which makes it necessary to use high cost materials [6, 7].

An alternative to thermal energy storage (TES) as sensible heat for storing energy in CSP plants is thermochemical energy storage (TCES) [8, 9] currently under research and development. TCES is based on the use of heat to carry out an endothermic reaction.

When this energy is required, the separately stored by-products of the reaction are brought together to carry out the reverse exothermic reaction, which releases the previously used heat for power production on demand. Main advantages of TCES are the potentially high energy density as well as the possibility of storing energy in the long term without losses. Moreover, in addition to the enthalpy of the chemical reaction, it is also possible to use the heat stored as sensible heat in the reaction products [4].

Among the diverse possibilities explored for TCES at large scale, one of the most promising technologies is the Calcium Looping (CaL) process, which relies on the carbonation/calcination reaction of CaO (Eq. (1)) [10].

$$CaO\ (s) + CO_2(g) \rightleftarrows CaCO_3(s), \qquad \Delta H_r^0 = -178\ kJ/mol \tag{1}$$

The energy density that can be potentially stored by the $CaO/CaCO_3$ system in terms of reaction enthalpy and density of the material (~3.2 GJ/m^3) is much higher than the sensible heat stored by solar salts currently used in CSP plants (~0.8 GJ/m^3) [3]. Limestone is a natural CaO precursor abundantly available at low price (~10 €/ton), non-toxic and with a high $CaCO_3$ content (close to 100%), albeit the CaO derived from its calcination may present a progressive deactivation with the number of cycles depending on reaction conditions [11].

Figure 1 shows a simplified flow diagram of a possible configuration for the CaL-CSP integration recently proposed elsewhere [12, 13], which is based in a closed CO_2 cycle for carbonation and power generation by means of a Brayton cycle. The process starts with the calcination of $CaCO_3$ in a calciner reactor using concentrated solar power as the heat source. Once the sensible heat from the streams exiting the calciner (CO_2 and CaO) is recovered, these products are stored separately. When required, the streams of CaO and CO_2 are transferred to the carbonator, wherein heat is recovered from the enthalpy of the carbonation reaction. In the carbonator, CO_2 reacts with CaO at conditions to shift the reaction towards exothermic carbonation to produce $CaCO_3$. The process is designed in such a way that the CO_2 mass flow rate entering in the carbonator is well above the stoichiometric need. Thus, the CO_2 in excess that exits the carbonator is used as fluid carrier to evacuate the heat released by carbonation and is looped through the closed power cycle for generation of electricity. The interested reader in further details is referred to [12, 13] for a rigorous mass-balance model of the plant taking into account the flow rates of solids and CO_2 streams between the carbonator and calciner and a rigorous energy

integration analysis. One of the main advantages of this integration is that the time and the conditions for storage are flexible and could be adjusted according to the energy demand [12, 13].

The calcination stage has an important role on the global efficiency of the process because for storing the highest amount of energy in sun hours decarbonation has to be fast and at the lowest possible temperature. The latter would allow the use of relatively cheap commercial solar receivers based on metal alloys thus reducing the cost and technological risk of the technology [14]. A possible choice to this end is to carry out calcination under a gas that could be easily separated from the CO_2 generated in this stage as could be He by using membranes [15, 16]. Moreover, the high thermal conductivity of He and high CO_2 diffusivity in this gas serves to speed up the calcination reaction [17]. This would help full calcination of the solids in short residence times at temperatures around 725ºC in the case of limestone [18]. However, the calciner technology is not yet fully developed. Small prototypes of solar chemical reactors have been proposed for the production of lime based on fluidized beds [19, 20], rotary kilns [21, 22] and cyclone atmospheric reactors [23]. In the CaL-CSP integration the effluent gas stream from the calciner must be cleared of particles before sending it to the membrane for He/CO_2 separation. Thus, a cyclone separator should be used for removing the particulates from the gas mixture.

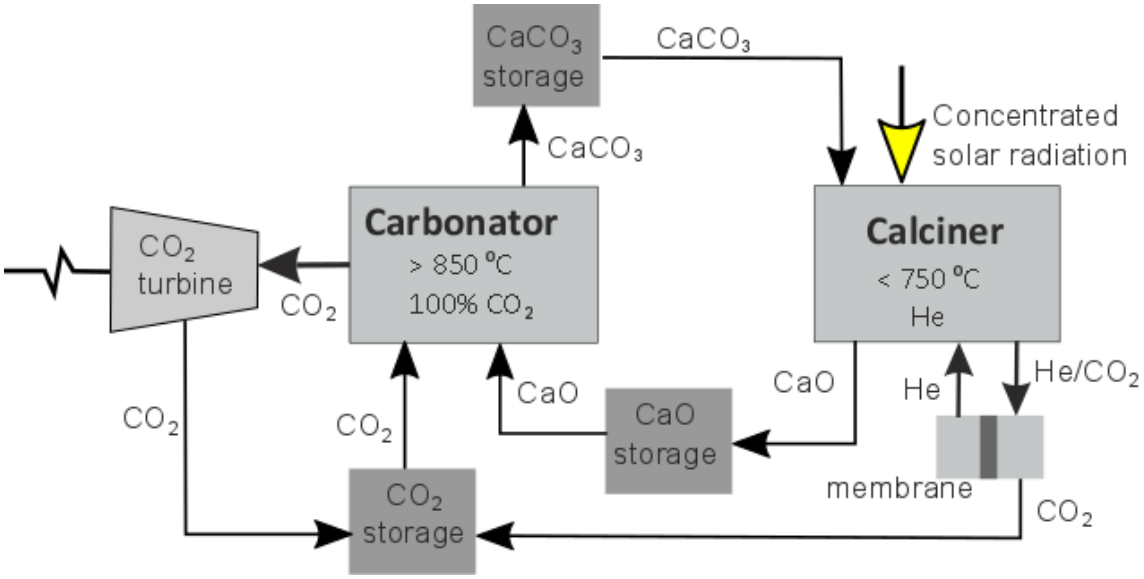

Figure 1. Flow diagram for the integration of the Ca-Looping process in Concentrated Solar Power plants with central tower technology for thermochemical energy storage. A detailed description can be found in [12].

According to process simulations the CaL-CSP integration may achieve a high thermoelectric global efficiency provided that the multicycle CaO conversion is kept above 0.5 after a large number of cycles [12]. In this integration scheme, the operation temperature in the carbonator would be around 850ºC or higher to optimize the thermoelectric efficiency and carbonation would be performed under pure CO_2. However, the global efficiency of the process decays notably if CaO conversion is decreased below 0.2 [12]. As shown in a recent work, the multicycle activity of limestone derived CaO is notably limited by pore plugging at these CaL conditions for particles of size above ~50 μm to be employed in practice [11]. The relatively low calcination temperature used at CaL conditions for CSP storage leads to a highly porous CaO skeleton. And these small pores become rapidly plugged by the thick layer of $CaCO_3$ that forms very quickly on the CaO particles' surface at the high temperature and high CO_2 concentration employed for carbonation [11].

The CaL process has been widely studied in the last years for CO_2 capture in fossil fuel power plants, which has been successfully demonstrated in large pilot-scale plants (1-2 Mwth) [24-26]. In this application the CaL process is carried out in two interconnected fluidized bed reactors. In the first one, carbonation of CaO solids takes place at temperatures near 650ºC under a ~15% CO_2 vol. atmosphere, which is the typical concentration of CO_2 in the flue gas. Then, the solids are circulated into a second reactor at temperatures between 900-950ºC under high concentration of CO_2 for the calcination stage. In that way, almost pure CO_2 can be extracted from this reactor for its subsequent compression and sequestration. After this stage, the regenerated CaO particles are circulated back into the carbonator for a new CaL cycle. Process conditions in the CaL cycle for CO_2 capture such as the high temperature and CO_2 concentration in the calciner lead to a drastic loss in the activity of CaO in short residence times as the number of cycles progresses. It must be stressed that the main limiting mechanism for the multicycle CaO activity at CaL conditions for CO_2 capture is diverse from that limiting the CaO activity at conditions for CSP storage. In the former case, the multicycle sorbent activity is hindered by the severe sintering of the regenerated CaO at the harsh calcination conditions, which yields a drastic loss of its surface area and therefore a drop of activity in short residence times [27-29].

Besides of limestone, an abundantly available Ca based material that could be used to store CSP by means of the CaL process is steel slag. In 2010, the production of this industrial waste in the European Union was around 21.8 millions of tons [30] of which about 76% is used for road construction, concrete manufacture and hydraulic energy and the rest is deposited in industrial dumps. According to the forecasted growth of the CSP technology, the huge amount of slag deposited in these dumps could be enough for its utilization as material for heat storage in CSP plants in 2050 [4, 31]. Steel slag has a similar heat capacity to solar salts and presents higher thermal conductivity (1.4 W/(m·K) for steel slag and 0.52 W/(m·K) for solar salt). Blast furnace slag is another industrial waste that could be used for heat storage [32-34]. According to the U.S. Geological Survey, in 2014 the U.S. blast furnace slag production was in the range of 16 to 22 million tons, with the ~70% used mainly as aggregate in concrete or feed for cement kilns [35]. Blast furnace slag is a by-product generated in the iron and steel industry when iron, coke and flux are melted in a blast furnace after the introduction of a reducer gas (usually CO). Then, the products, iron and flux impurities, are conducted to the sprue of the melting pot for their separation by density. The slag comes out of the crucible at temperatures around 1500ºC, and materials with different physical properties are obtained depending on the technique employed for cooling it. The ground granulated blast furnace slag is produced by fast cooling of the liquid slag with large quantities of water, which yields a sand-like vitreous material. Blast furnace slag can also be cooled down slowly by ambient air in slag pits, forming a crystalline rock-like material but more porous than natural minerals. Valorisation of steel slag has been in fact recently proposed for the storage of CSP in the form of sensible heat [4] with a lower estimated cost of storage as compared to solar salts (1.1€/Kwh for steel slag compared to 5.2€/Kwh for solar salt) [4]. On the other hand, steel slag can be transformed into a CaO precursor by a simple process basically consisting of acetic acid treatment and its CaL performance at conditions for CO_2 capture has been reported elsewhere [36-38]. Hu et al. [39] and Ridha et al. [40] have recently reported a comparison of several CaO based sorbents obtained by modifying limestone with diverse acids, which showed superior performance at CaL conditions for CO_2 capture. Nevertheless, such treated sorbents react preferentially with SO_2 present in the coal combustion gas causing their capture capacity to drop severely [40]. Thus, a main advantage of using the CaL process in CSP plants would be the absence of SO_2 in the reacting gas. The present manuscript is focused on analysing the multicycle behavior of

diverse samples of steel and blast furnace slags modified with acetic acid for thermochemical energy storage in CSP plants by means of the CaL process.

2. Materials and methods

Electric arc furnace slag (steel slag) samples were supplied to us by Acerinox Europe S.A.U (Los Barrios, Spain) and Siderúrgica Sevillana, S.A. (Alcalá de Guadaira, Spain). Blast furnace slag samples were received from Erdesa, S.A. (Avilés, Spain). The sample from Acerinox Europe consists of a black powder with particle size ≤ 750μm. Siderúrgica Sevillana supplied us with two steel slag samples labelled as "low iron content" and "high iron content" with particle size ≤2 mm and between 2 and 6 mm, respectively. Finally, the samples from Erdesa consisted of three blast furnace slags: a white powder of granulated slag, granulated slag with 8% of $CaCO_3$ added, and a grey slag with particles of around 2 mm size. Samples with initially large particles (≥1 mm) were subjected to a mechanical milling treatment in order to reduce their size and facilitate their subsequent acetic acid treatment. Mechanical milling was performed with a Fritsch Pulverisette 6 (centrifugal ball mill, Idar-Oberstein, Germany) in the case of blast furnace slag, and with a Fritsch Pulverisette 7 (planetary ball mill, Idar-Oberstein, Germany) for the slags received from Siderúrgica Sevillana. The use of the latter high energetic mill was required due to the hardness of the particles. After particle size reduction with the planetary ball milling the samples were sieved using a 320 μm pore size sieve.

The acetic acid treatment of the raw samples was aimed at obtaining calcium acetate as CaO precursor. It consisted of mixing the powder with an acetic acid (VWR Chemicals, 99.9% purity) aqueous solution (25 wt%) by a ratio of 1 g of powder sample per 50 mL solution. In the case of the third blast furnace slag received from Erdesa, the acetic acid concentration had to be increased to 50 wt% and the ratio between sample and solution to 2 g per 50 mL. The mixture was magnetically stirred at room temperature until the solids were dissolved for 1-2 h and then left to rest. After the stirring and resting step, a segregation of two phases was observed, which consisted of a gel and a liquid. From this point, two batches of samples were prepared.

For the first batch, the mixture was heated at 120ºC for 2 hours to evaporate the solvents, and the solids obtained were grinded in an agate mortar. For the second batch, an

intermediate step was introduced which consisted of separating the gel phase from the liquid by filtration. Once the gel phase was removed, the liquid was heated at 120ºC for 2 hours, and the solids grinded in the agate mortar.

The samples obtained after just the acetic acid treatment were labelled as A1 (Acerinox sample); E1, E2, E3 (Erdesa samples); S1, S2 (Siderurgica Sevillana samples). The samples resulting from removing the gel phase by filtration were labelled in the same way with an intercalated "F" (e.g. AF1 for sample 1 from Acerinox).

Elemental composition of the raw powdered samples obtained after the treatment was analysed by X-ray microfluorescence (XRF) using an Eagle III Micro XRF instrument (EDAX, New Jersey, USA) equipped with an X-ray anticathode 50W rhodium tube and an energy dispersive X-ray detector and with a maximum operating potential of 40 keV and 1 mA. X-ray diffraction measurements were made using a Panalytical X'Pert Pro diffractometer working at 45V and 40mA with Cu-Kα radiation and equipped with an X'Celerator detector and a graphite diffracted beam monochromator. Besides, a Rigaku MiniFlex 600 instrument was employed equipped with a Cu detector, working at 40kV and 15 mA, using a Cu-Kα radiation. Scanning electron microscopy (SEM) analyses of pretreated and cycled samples were performed using a Hitachi S5200 HR microscope. Pore size distributions were measured by means of Hg porosimetry using an Autopore IV instrument and by N_2 sorption at 77 K (Micromeritics ASAP 2020).

Carbonation/calcination cycles were carried out using a thermogravimetric analyser (TGA) Q5000IR (TA Instruments, Crawley, UK) equipped with a high sensitive microbalance for accurate measurement of very small mass losses (< 1μg). The furnace of this instrument has four symmetrically-disposed infrared halogen lamps that ensures uniform heating and allows to carry out fast and controlled temperature ramps up to 300ºC/min with 1ºC accuracy. The water-cooling system provides an efficient heat-sink and facilitates controlled cooling rate from 1200ºC to room temperature. The sample is placed inside a SiC enclosure surrounded with gold elliptical reflectors that minimizes undesirable effects of heat transfer phenomena and the thermocouple is located below and close to the sample holder to register the temperature.

TGA experiments were initiated by calcination of the sample (precalcination stage), which was followed by 21 carbonation/calcination cycles. The precalcination stage was carried out by increasing the temperature at either 10ºC/min up to 650ºC under a pure He

atmosphere. Then, the temperature was rapidly increased to 850ºC at 300ºC/min and the atmosphere was changed to pure CO_2 to introduce the carbonation stage. After this stage, the sample was calcined again at 650ºC under He for CaO regeneration. The residence time was fixed to 5 minutes for both the carbonation and calcination stages. Between stages, a 5 min intermediate step at 150ºC was introduced for simulating the storage stage of the material after extraction of sensible heat. These conditions would mimic the practical conditions for integrating the CaL process in the CSP technology, which involve cooling and storing the solids between the periods of load and discharge [12]. Small amounts of samples (about 10 mg) were employed in order to avoid effects caused by gas diffusion resistance through the sample, which could be relevant for sample masses above 40 mg [41]. With the aim of comparing the performance of CaO precursors obtained from the slags with natural limestone, conversion data for limestone reported in [18] will be also shown in the present manuscript. In that work, the TGA experiment on a limestone sample was carried out at similar conditions to those used in the present work: calcination at 725ºC under pure He atmosphere and carbonation at 850ºC under pure CO_2 atmosphere with 5 min as residence times. As will be seen below calcination of the treated slag samples was achieved at a substantially lower temperature (650ºC), which represents already a significant benefit as compared to limestone that requires a minimum temperature of 725ºC for calcination to be quickly attained.

3. Results and discussion

Elemental composition results of the samples obtained after treatment measured by XRF analysis are summarized in table 1. As can be seen, a general result is that the intermediate filtration step serves to increase the Ca content while the Si content was notably reduced.

Sample	O	Ca	Si	Al	Fe	Mg	Mn	Cr	Other
A1	36.29	37.09	13.54	0.70	0.58	1.99	5.07	3.87	1.07
AF1	29.35	54.15	0.85	0.54	0.93	3.05	7.09	3.53	0.92
S1	36.07	35.97	7.42	4.12	4.65	9.00	1.28	0.16	1.33
SF1	31.91	48.54	0.41	3.95	4.12	7.95	1.51	0.06	1.55
S2	35.08	23.48	6.80	3.96	21.55	4.91	2.49	0.37	1.37
SF2	30.39	51.77	0.14	1.71	6.19	5.74	2.8	0.08	1.18
E1	40.38	31.09	16.05	5.91	0.21	4.27	0.26	0.01	1.78
EF1	31.65	54.78	0.35	6.38	0.33	4.69	0.62	-	1.2
E2	39.36	34.59	14.76	5.30	0.23	3.74	0.25	-	1.72
EF2	32.09	53.5	0.38	7.77	0.46	4.07	0.5	-	1.23
E3	40.58	30.09	16.65	5.61	1.21	3.67	0.27	-	1.81
EF3	32.92	50.61	1.31	7.79	1.57	3.51	0.58	0.05	1.66

Table 1: XRF elemental composition of the samples obtained from steel and blast furnace slag treated with acetic acid and those obtained employing the intermediate filtration step.

Due to the complex oxides present in the raw samples and the absence of free CaO, the application of an acid pretreatment was needed to obtain a CaO precursor after calcination [42, 43]. The results of these treatments slightly differ from one slag to another as can be interpreted by the XRD patterns shown below, in which calcium acetate or calcium magnesium acetate with clearly defined peaks [44-47] are revealed as the major phases. SEM analysis allowed us to observe the rod-shape microstructure typical of these acetates [46-48] as will be seen ahead. Thermal decomposition of the pretreated samples, consisting mostly of calcium acetate and calcium magnesium acetate, was performed under He flow in the Q5000I instrument at constant heating rate (10ºC/min) for quantifying the mass % that would correspond to $CaCO_3$ and CaO in the treated slag and the relative amount of impurities. Next sections are devoted to XRD, thermogravimetric

and SEM characterization of the synthesized samples after which multicycle activity results will be shown and discussed.

3.1. Acerinox steel slag

Characterization of Acerinox samples after treatment by means of XRD analysis (Fig. 2) shows that hydrate calcium acetate is the major phase present both in A1 (a) and AF1 (b), with a secondary phase of calcium magnesium acetate. The minor presence of traces of other metallic oxides or compounds in crystalline form was not detectable by means of XRD.

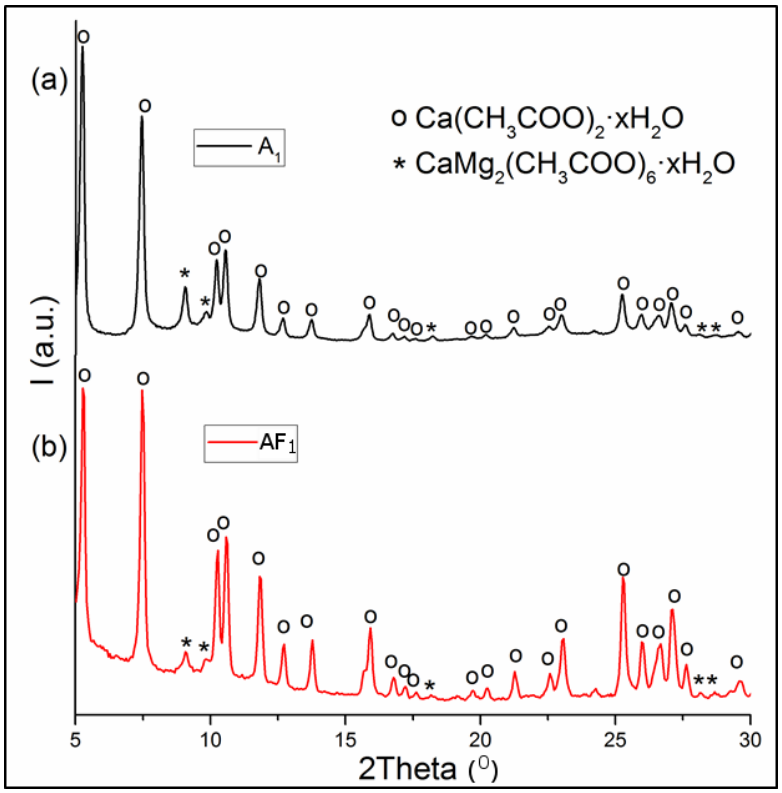

Figure 2. XRD patterns measured for samples received from Acerinox Europe S.A.U. after treatment with acetic acid, A1 (a), and after acetic acid treatment that included the filtration step AF1 (b). As indicated, the reflection peaks reveal the presence of calcium acetate as the dominant phase. The 2Theta measured range was 5-90º. Only the interval 5-30º containing the most relevant reflection peaks is shown.

Figure 3 shows thermal decomposition thermograms of the A1 and AF1 samples. It is seen that thermal decomposition of calcium acetate, as a main phase present in the samples, takes place in three stages as well-known from previous studies [44, 47]. We

observe also a fourth fast stage due to the presence of a small amount of calcium magnesium acetate [45, 49]. The first stage is due to dehydration of the precursors in two steps, from room temperature to 200ºC approximately, which leads to a first mass loss of about 17 mass % for A1 and 12 mass % for AF1. The second mass loss is due to the decomposition of calcium acetate and the minor phase of calcium magnesium acetate (Eq. (2)), which yields acetone to obtain the calcium and magnesium carbonates at temperatures between 345ºC and 420ºC for A1 and 430ºC for AF1, leaving the sample mass at 64 and 60 mass %, respectively,

$$Ca(CH_3COO)_2 + CaMg_2(CH_3COO)_6 \rightarrow 2CaCO_3 + 2MgCO_3 + 4(CH_3)_2CO\uparrow \quad (2)$$

The resulting $MgCO_3$ remains stable under the inert atmosphere for a short time and decomposes almost immediately to MgO at 455ºC and 470ºC for A1 (56 mass %) and AF1 (52 mass %), respectively (Eq. (3)).

$$CaCO_3 + MgCO_3 \rightarrow CaCO_3 + MgO + CO_2\uparrow \quad (3)$$

The final stage consists of $CaCO_3$ decomposition (Eq. (4)) and takes place between 550ºC and 650ºC for A1, and between 600ºC and 670ºC for the AF1 sample. The mass loss for A1 is about 13 mass % whereas for AF1 is about 18%. Since SiO_2 was removed in AF1 by filtration there is a higher amount of CaO in this sample.

$$CaCO_3 + MgO \rightarrow CaO + MgO + CO_2\uparrow \quad (4)$$

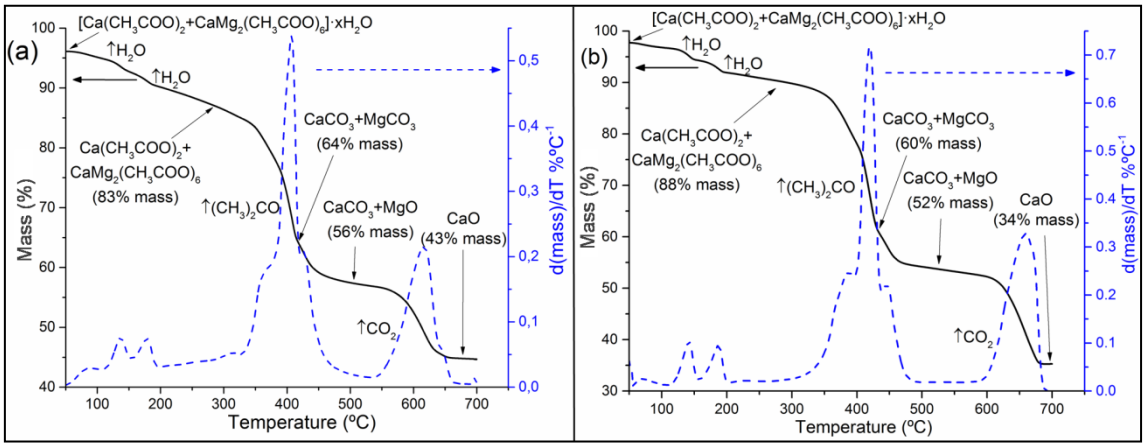

Figure 3. Mass percentage and its derivative with temperature as a function of temperature during thermal decomposition under a pure He atmosphere at constant heating rate (10ºC/min) of the treated Acerinox steel slag samples A1 (a) and AF1 (b).

As seen in the SEM micrographs (Fig. 4), the treated samples show the typical rod-shape morphology of calcium acetate and calcium magnesium acetate crystals [46-48, 50]. The presence of other metal oxides (M_xO_y), composed mainly by Si (only in the case of A1), Mn, Mg and Cr according to the XRF analysis can be also appreciated in the form of aggregated nanoscale sized agglomerates distributed on the surface of the acetate rods.

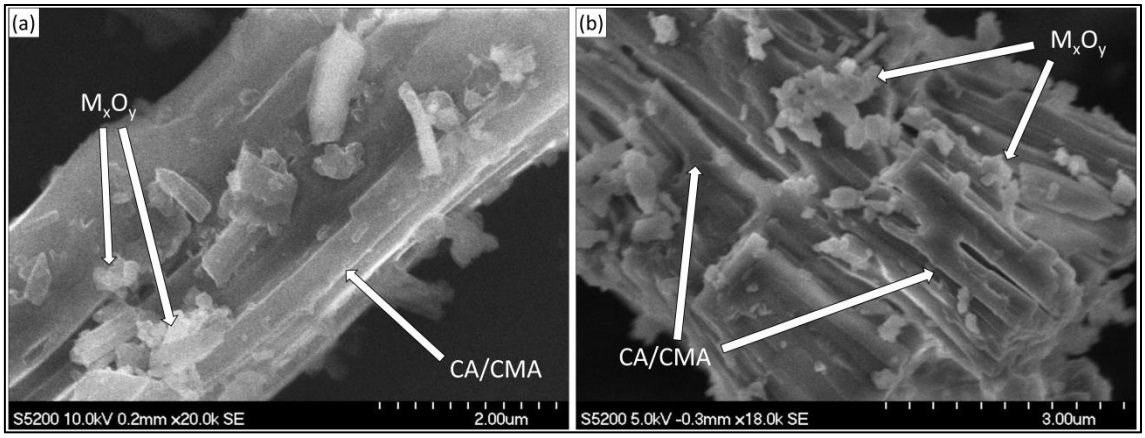

Figure 4. SEM micrographs of Acerinox samples obtained by acetic acid treatment, A1 (a), and AF1 (b).

3.2. ERDESA blast furnace slags

Blast furnace slags were divided in two sub-groups, one for the amorphous (as inferred from the broader peaks in the DRX scans) slags that were subjected in the industry to a fast cooling treatment, which includes the raw granulated slag and the one with the addition of 8 % of $CaCO_3$ (to be employed for concrete production); and the slag with a higher crystallinity, which resulted from a slow cooling treatment in the industry. The similar mass % of metallic elements present in the raw slags of both groups indicates a common source, thus the samples only differed in the cooling treatment. The Ca mass % of these samples, around 31% (34% in the sample with 8% $CaCO_3$ added), is lower than that corresponding to the Acerinox steel slag, which could be a relevant issue for their multicycle carbonation behaviour. XRF analysis shows that Si and Al are present in the samples in high amounts (about 16 and 5 mass %, respectively). Alumina is known to react with calcium carbonates to form calcium aluminate at high temperatures [51], which could remove a relevant amount of active CaO for carbonation from the sample. On the

other hand, calcium silicates could be also formed but by a small amount at the CaL operation temperatures [52]. As shown in previous works the presence of silica grains confers thermal stability to the composite, which serves to mitigate the severe sintering suffered by the sorbent at the harsh calcination conditions for CO_2 capture [36, 52]. Other metallic elements are present in the samples such as Mg, Fe or Ti are expected to remain inert through the carbonation/calcination cycles.

Fig. 5 shows X-ray diffractograms of the three compounds obtained by acetic acid treatment on amorphous blast furnace slag (E1), the 8 % $CaCO_3$ added slag (E2) and the crystalline blast furnace slag (E3). The first slag, produced after a fast cooling treatment, had the appearance of an amorphous white fine powder. Once treated with acetic acid (sample E1 in Fig 5a) it shows the presence of calcium acetate and calcium magnesium acetate as major phases. In the compound E2 the XRD pattern shows the same crystalline phases (Fig 5b). Besides, minor peaks were detected that correspond to the metal oxides present in the slag. A calcium acetate and calcium magnesium acetate solid mixture was obtained also along with secondary phases from the crystalline blast furnace slag as seen in Fig 5c.

Fig. 6 shows the thermograms recorded from thermal decomposition of the compounds obtained from the treated blast furnace slags. Acetate precursors synthetised from the amorphous slag (Fig 6a), amorphous slag with 8% $CaCO_3$ added (Fig 6b), and crystalline slag (Fig 6c) exhibit thermogravimetry patterns similar to those observed and previously reported for the mixture calcium acetate/calcium magnesium acetate [45]. The initial ~20 mass % loss that corresponds to dehydration takes place up to 280 - 300ºC depending on the compound. The second mass drop is caused by the decomposition of acetates between 350 and 430 ºC,which releases acetone to yield $CaCO_3$ and $MgCO_3$ (Eq. (2)), remaining a mass % of around 60% for a short interval of temperatures due to the subsequent fast decomposition of magnesium carbonate into MgO (Eq. (3)), which ends at about 460 - 470ºC (~52 – 55 mass % is left). The last mass loss between 580 and 650 ºC (about 10 mass %) is caused by $CaCO_3$ decarbonation.

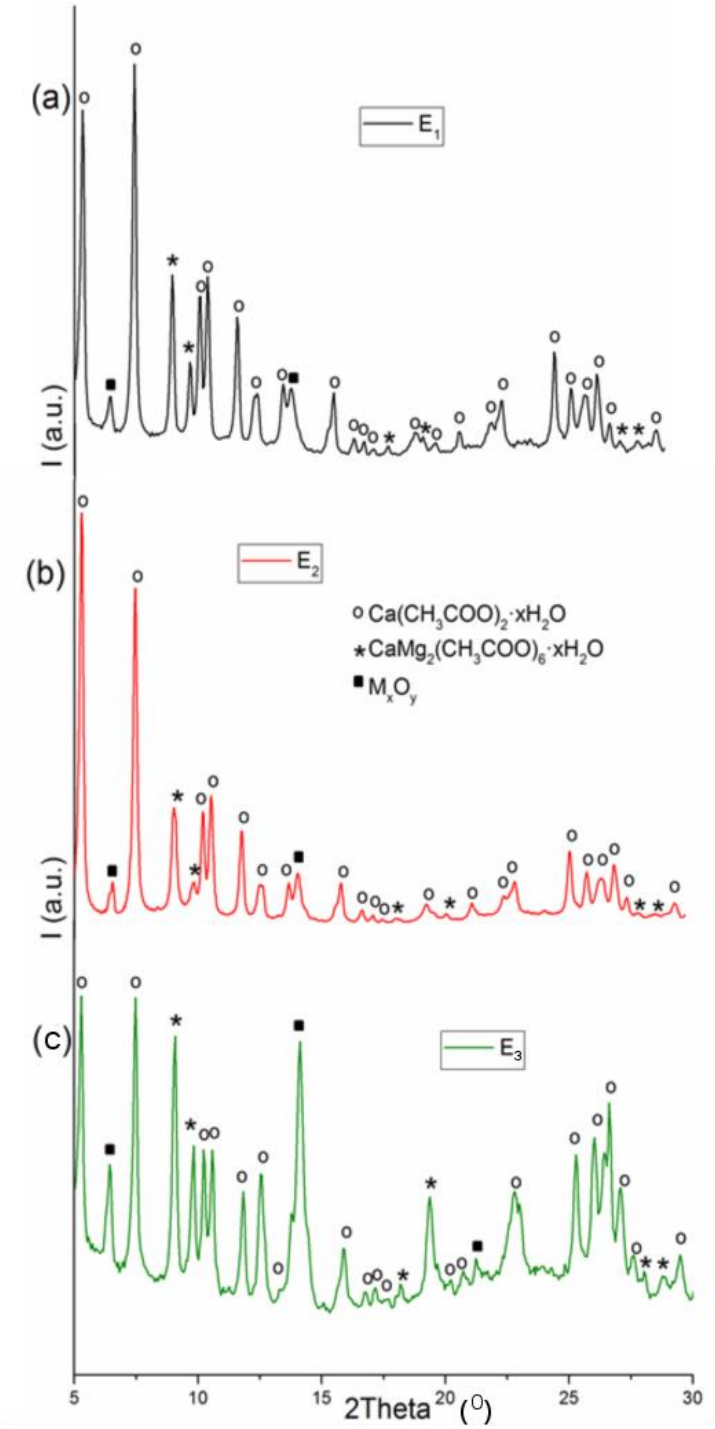

Figure 5. X-ray diffraction patterns obtained for the ERDESA blast furnace slag samples treated with acetic acid: amorphous slag, E1 (a), amorphous slag with 8% $CaCO_3$ added, E2 (b), crystalline slag, E3 (c).

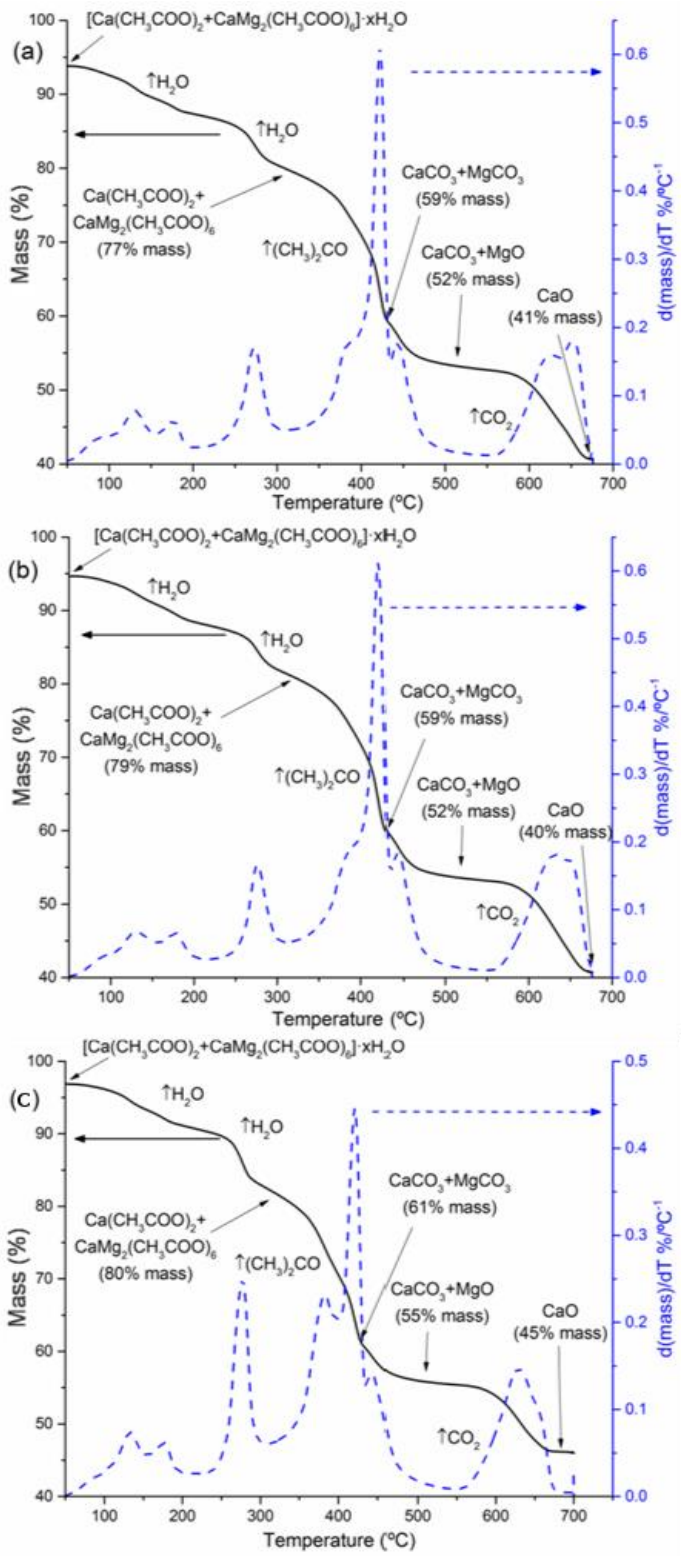

Figure 6. Thermal decomposition during heating at 10ºC/min under He of the compounds obtained by acetic acid treatment of the Erdesa blast furnace slag samples: E1 (a), E2 (b), E3 (c). Mass loss (%) and its derivative are plotted as a function of temperature.

SEM micrographs in Fig. 7 illustrate the morphology of the compounds obtained after the acetic acid treatment on the amorphous and crystalline blast furnace slags. The treatment performed on E1 (Fig. 7a) lead to the formation of small rods typical of calcium acetate and calcium magnesium acetate [50]. It is also observable the presence of metal oxide impurities that would mostly consist of SiO_2 according to the XRF analysis (Table 1). Larger crystals of calcium acetate/calcium magnesium acetate are visible in the case of the amorphous slag with 8% $CaCO_3$ added (Fig 7b) with also metal oxide grains distributed on the surface of the grains. The acid treatment applied on the crystalline slag yields also calcium acetate and calcium magnesium acetate crystals but in the form of thin sheets, which are covered with some impurities (Fig 7c). Thus, the typical rod-shape form of the pure acetates reported elsewhere [50] is seen in our work only when these acetates are synthesized from the amorphous slag.

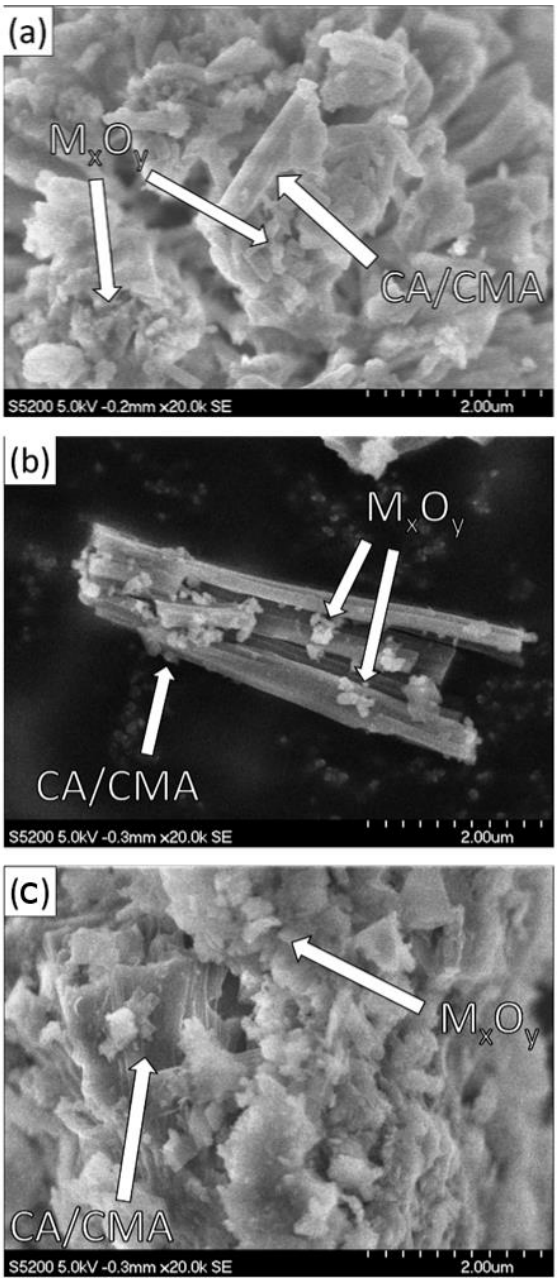

Figure 7. SEM micrographs of the compounds blast furnace slags treated with acetic acid: E1 (a), E2 (b), E3 (c). The presence of calcium acetate (CA), calcium magnesium acetate (CMA) and metallic oxide grains is indicated.

3.3. Siderúrgica Sevillana steel slag

XRD patterns (Fig. 8a and b) of the treated steel slag samples from Siderúrgica Sevillana, S1 and S2 illustrate the presence of calcium acetate and calcium magnesium acetate as main crystalline phases. Other peaks correspond to minor secondary phases (labelled as

M_xO_y). In these samples the relative intensity of the peaks corresponding to the calcium magnesium acetate phase is notably increased, which indicates a higher Mg content.

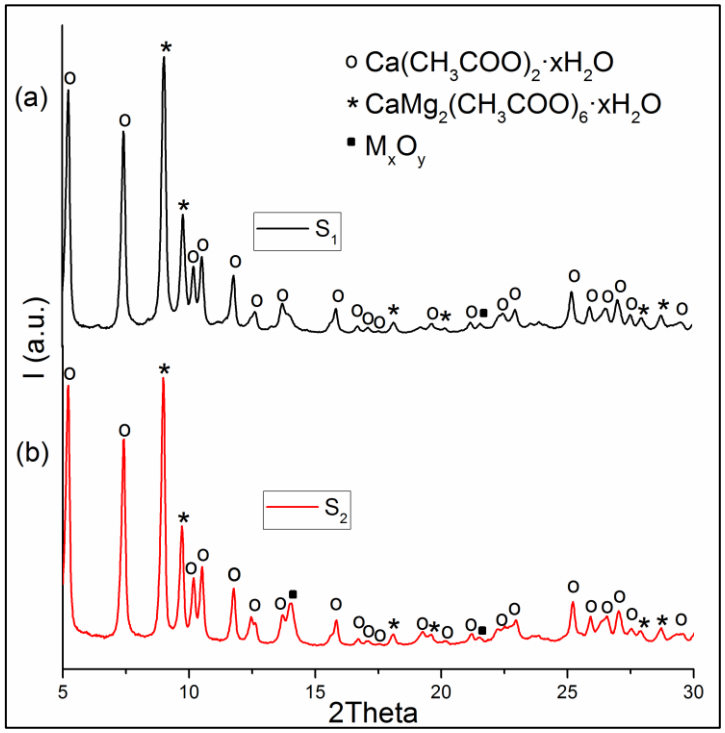

Figure 8. X-ray diffractograms of samples received from Siderúrgica Sevillana after the treatment performed with acetic acid, S1 (a) and S2 (b). Main peaks indicate the dominant presence of calcium acetate and calcium magnesium acetate.

Thermal analyses performed on the treated steel slag samples S1 (Fig. 9a) and S2 (Fig. 9b) show the typical decomposition thermogram reported for pure calcium acetate and calcium magnesium acetate [44, 45, 48, 49] with small variations due to the presence of impurities. The first mass loss corresponds to dehydration (~15 mass % loss). The release of acetone in calcium acetate/calcium magnesium acetate decomposition (Eq. (2)) takes place between 340ºC and 420ºC, which leads to a mixture consisting of $CaCO_3$ and $MgCO_3$. In the third step, decomposition of $MgCO_3$ occurs up to 470ºC, yielding $CaCO_3$ and MgO (Eq. (3)), which is stable until about 600ºC. The last stage takes place up to 650ºC, releasing CO_2 from decarbonation of $CaCO_3$ (Eq. (4)). As seen in Figs. 9a-b, the samples before the last decomposition (consisting of $CaCO_3$ plus metal oxides) present a 49 and 54 mass % of the initial mass while the mass after decomposition (CaO with

oxides) remains at 39 and 45 mass % for S1 and S2, respectively. This difference between both samples can be attributed to the high content of Fe in S2.

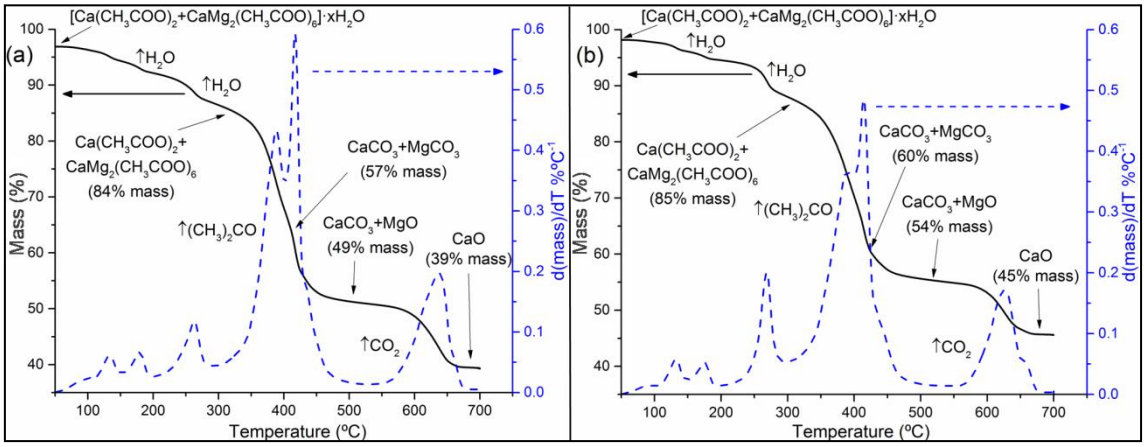

Figure 9. Mass percentage and its temperature derivative as a function of temperature during thermal decomposition of Siderúrgica Sevillana treated steel slag samples S1 (a) and S2 (b), performed under He atmosphere at constant heating rate of 10ºC/min.

SEM micrographs of Siderúrgica Sevillana treated steel slag samples are shown in Fig. 10 illustrating also the typical rod shaped grains of calcium acetate and calcium magnesium acetate [46-48]. Besides, impurities in the form of metal oxides (M_xO_y) nanoscale size agglomerates can be clearly appreciated in the surface. In this case, the microstructures of the S1 and S2 samples do not present relevant differences in spite of their diverse elemental composition, especially regarding the higher Fe content in S2.

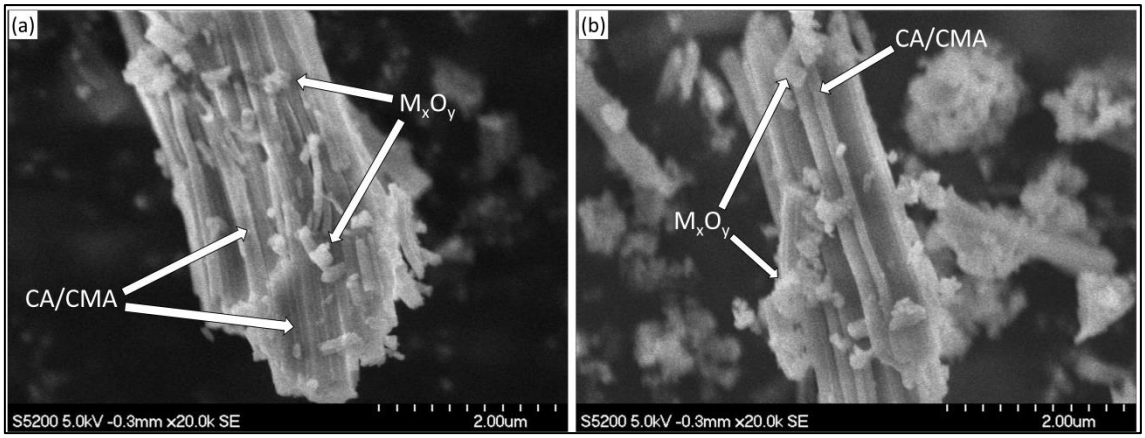

Figure 10. SEM micrographs of Siderúrgica Sevillana treated samples with low Fe mass %, S1 (a) and high Fe mass %, S2 (b). Calcium Acetate (CA) and Calcium Magnesium Acetate (CMA) grains as well as metal oxide impurities are indicated.

3.4. CaL-CSP multicycle conversion

The multicycle performance of the CaO precursors prepared from the diverse steel and blast furnace slags was assessed at CaL conditions for CSP storage. As detailed above (Fig. 1) these conditions involve carbonation at high temperature (850ºC in our tests) under pure CO_2 and calcination at a relatively low temperature under He. In the case of limestone, calcination is completely in short residence times under He at about 725ºC [18] whereas for the steel slag treated samples fast calcination was fully achieved at around 650ºC as seen in the previous sections.

A more practical parameter than CaO conversion to compare the multicycle performance of diverse materials is the effective conversion X_{ef}, which is defined as the ratio of mass of CaO converted at the end of the carbonation stage to the total mass of the material before carbonation including impurities that remain inert at the carbonation conditions. Thus, this parameter serves to take into account the presence of inert solids in the slags that do not participate into the carbonation. Figure 11 shows the effective conversion measured as a function of the cycle number for the treated Acerinox steel slag sample A1 without filtration and for the sample obtained by applying filtration as intermediate step AF1. Data measured for limestone (of similar particle size) are plotted for comparison. As may be seen, the effective conversion of sample A1 remains at relatively low although stable values (close to 0.2) from the first cycle. Conversion of limestone in the first cycles is high but it drops notably with the number of cycles as due to pore plugging (see for [11] for a detailed discussion). On the other hand, the sample AF1 exhibits high and stable values of effective conversion from the first cycle (close to 0.6). A typical tThermogram showing the time evolution of weight and temperature during precalcination and 1st carbonation/calcination cycle is also shown in Fig 11. As can be seen in this thermogram carbonation occurs mainly in a first fast phase, which is controlled by the reaction kinetics as might be expected from the high carbonation temperature [26].

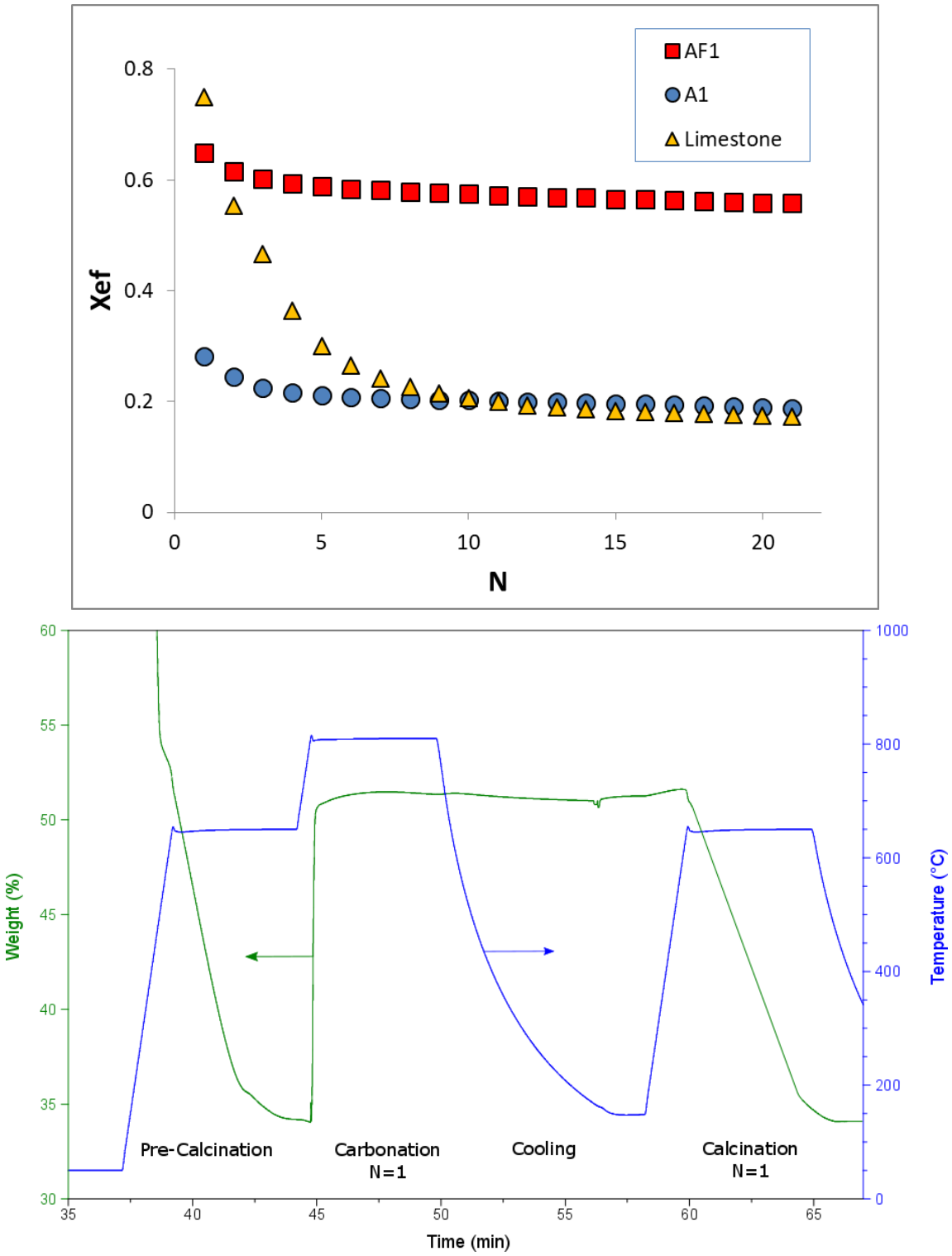

Figure 11. Top: Multicycle effective conversion measured for the acetic acid treated Acerinox steel slag samples A1 and AF1, and for limestone at CaL conditions for CSP storage (carbonation under CO2 at 850ºC and calcination under He, both stages for 5 minutes). In the case of limestone calcination was achieved at 725ºC whereas it was attained at 650ºC for the steel slag derived samples. Bottom: Thermogram showing the time evolution of weight and temperature during precalcination and 1st carbonation/calcination cycle (sample AF1).

Fig. 12 shows data on the multicycle effective conversion measured for all the treated slags. Results for the acetic acid treated samples are plotted in Fig 12a whereas Fig 12b shows data on the samples obtained by applying filtration to these samples as an intermediate step. As observed for the Acerinox AF1 sample (Fig. 11), filtration generally leads to a significant improvement of the effective conversion. All the samples derived from Acerinox and Siderurgica Sevillana steel slags with the intermediate filtration step exhibit high and stable values of effective conversion.

As derived from XRF analysis (Table 1) the main effect of filtration is to remove the silica particles present in the slags by a high percentage. Thus, it may be inferred that silica particles hinder the multicycle performance of the samples at CaL conditions for CSP storage. This apparently surprising result has been recently reported also for silica/CaO composites obtained from a physical mixture of limestone and a commercial nanoscale silica [53] and can be explained from the main limiting mechanism at the CaL conditions specific for CSP storage. Carbonation at high temperature under high CO_2 concentration leads to a very quick built up of a thick $CaCO_3$ layer on the surface of the particles that would block the access of CO_2 to the inner porous skeleton. Pore plugging would be favoured by the low calcination temperatures, which lead to a porous solid structure. Porosity is also enhanced by the presence of silica as shown in previous works focused on the performance of the material at conditions for CO_2 capture [52, 54]. The multicycle performance of CaO at CaL conditions for CO_2 capture is critically limited by CaO sintering at the harsh calcination conditions used in this application, which is mitigated by the presence of silica that confers thermal stability to the composite. This porosity enhancement effect of silica for the steel slags synthesized in our work can be seen in Fig. 13, which shows the pore size distribution measured for A1 and AF1 (with reduced Si content) after calcination. In the case of CaL conditions for CSP storage such effect of silica plays an adverse role as smaller pores are more prone to be plugged.

Other works reported in the literature show also that a higher porosity results in a drop of the multicycle CaO activity at CaL conditions similar to ours. Thus, Lu et al. [55] tested a number of CaO-based sorbents at calcination conditions involving a relatively low calcination temperature (700 °C) under He and carbonation under high CO_2 concentration. In agreement with our observations, Lu et al. observed that the addition of nanosilica did impair the CaO carbonation activity at these CaL conditions. Remarkably, the pore size distribution after many cycles was seen to remain stable for a Ca-acetate-

based sorbent, which showed a high and stable multicycle conversion. Likewise, Pinheiro et al. [56] tested several CaO-based sorbents at similar CaL conditions and observed a poor performance for the samples with increased BET surface area and smaller pores, indicating that pore plugging was the main mechanism limiting carbonation when calcination is carried out a relatively low temperature.

In regards to the treated blast furnace slag samples, it is seen that the effective conversion decays with the cycle number and drops to a low value after 20 cycles even for the samples obtained with the intermediate filtration step (EF1, EF2, EF3 in Fig. 12b). A possible explanation to this behaviour can be made on the basis of the high Al content of these blast furnace slags, which is increased in the liquid phase recovered after filtration (Table 1). As well-known from previous studies on Ca based materials doped with Al, calcium aluminates are irreversibly formed at temperatures above 600ºC, which would withdraw active CaO for carbonation from the sample.

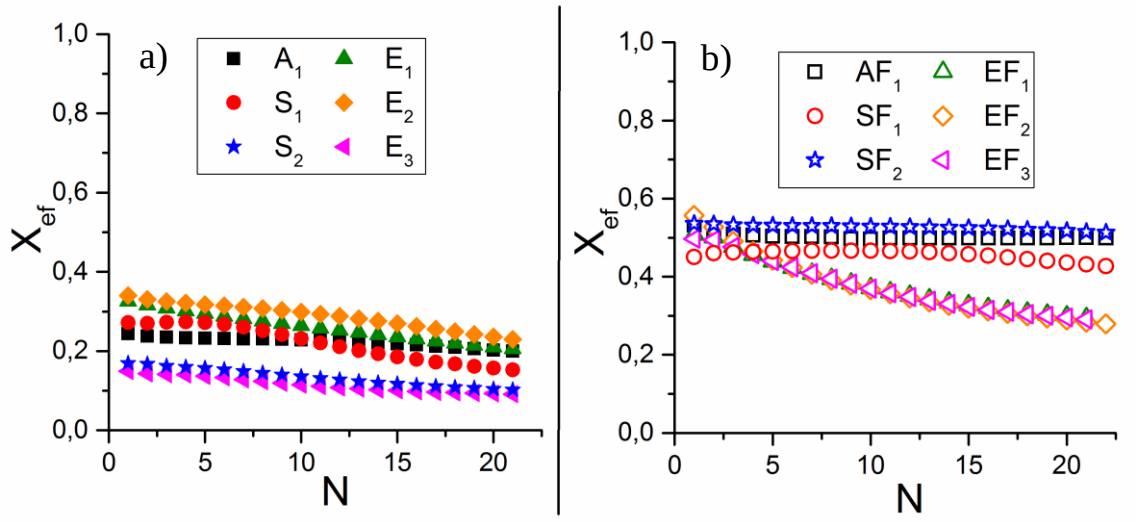

Fig. 12. Effective conversion as a function of the cycle number for the steel slag and blast furnace samples prepared by acetic acid treatment (a) and the acetic acid treatment that included the filtration step (b).

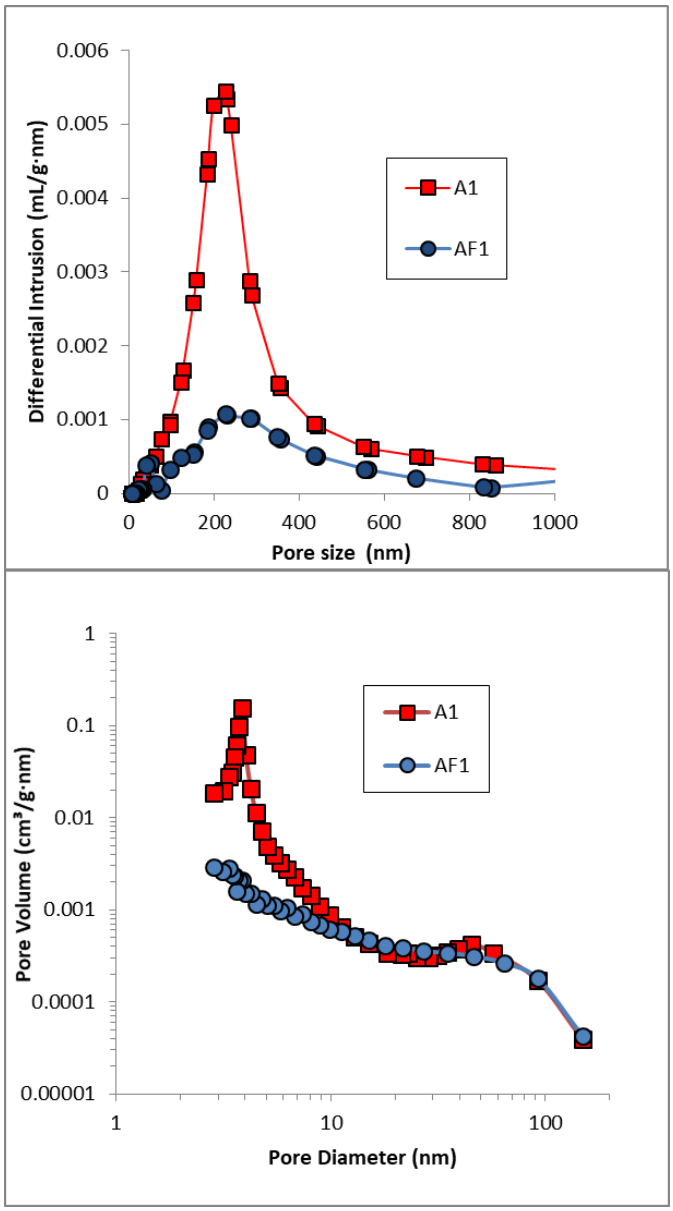

Figure 13. Pore size distribution (top: measured by means of Hg porosimetry; bottom: measured by N_2 desorption at 77 K) of calcined samples of acetic acid treated Acerinox steel slags. Data are shown for the treated slag directly obtained by the acetic acid treatment (A1) and for the sample oobtained by applying filtration as an intermediate step of the process (AF1).

Our results suggest that the multicycle performance at CaL conditions for CSP storage of the calcium and magnesium acetates derived from either steel or blast furnace slags would be enhanced as long as these compounds are extracted as pure as possible. The presence of metal oxide impurities, especially Si and Al oxides, would hinder the multicycle conversion of these materials at the conditions of our tests. On the other hand, since the Tamman temperature for $CaCO_3$ (533 ºC) is much smaller than the carbonation

temperature used at CaL conditions for thermochemical energy storage (850ºC), a rather low porosity should be expected for the $CaCO_3$ formed in the carbonator and therefore a high degree of crystallinity as a consequence of thermal annealing. This may be seen in Fig. 14 where SEM micrographs are shown for the E1 and EF1 samples after being cycled (ending in carbonation). In a previous work [57] we tested the effect of limestone annealing by prolonged isothermal heating (850 ºC for 12 h in a CO_2 atmosphere) on its CO_2 capture capacity. The results indicated only a slight decrease of the capture capacity while thermal annealing hardened the solid, which can be an advantage. A further effect of annealing would be to slow down $CaCO_3$ calcination as crystal defects would promote the nucleation of decarbonation and CO_2 diffusion [58]. In the present case, the presence of impurities in steel slag up to a certain level would serve to mitigate this effect which would allow calcination to be initiated at a relatively low temperature at a fast rate.

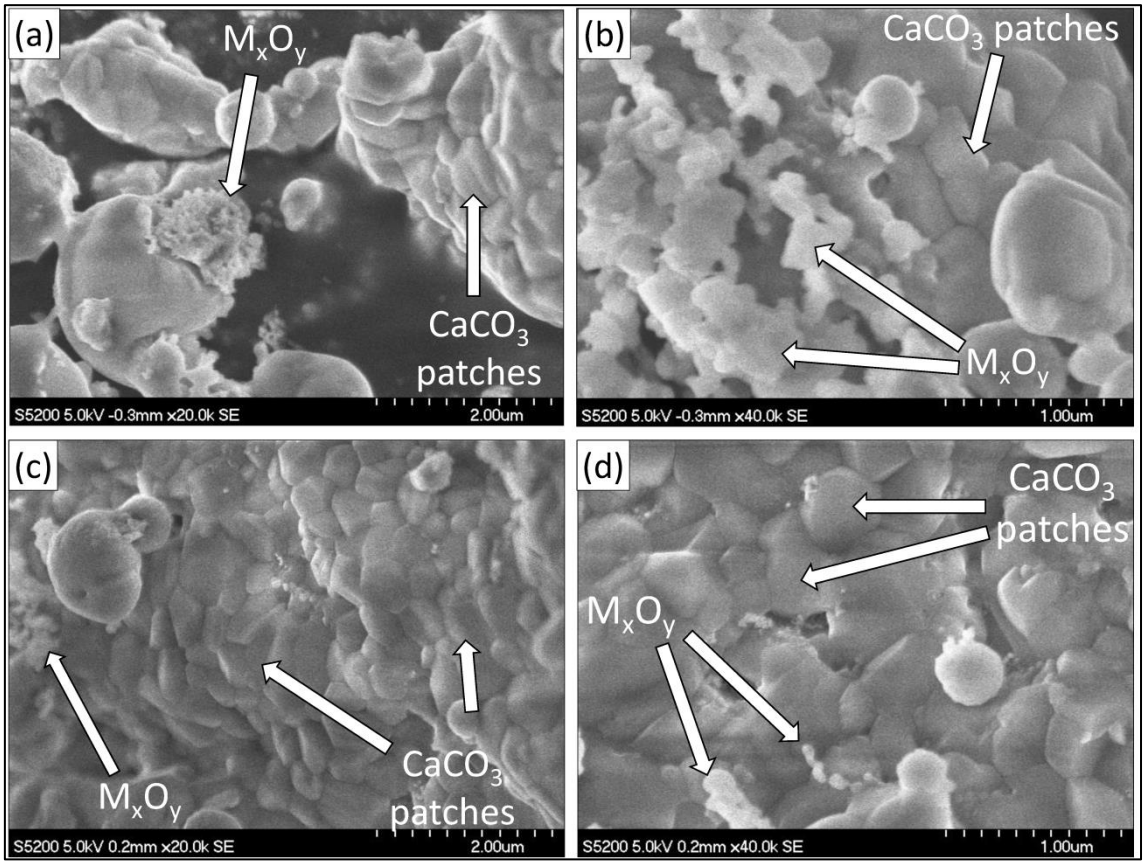

Figure 14. SEM micrographs of E_1 (a and b) and E_2 (c and d) pretreated slag samples after been subjected to 21 cycles of calcination at 650ºC under He and carbonation at 850ºC under CO_2.

4. Conclusions

This work analyses the multicycle Calcium-Looping activity at conditions for thermochemical energy storage in Concentrated Solar Power plants of Ca-based materials derived from acetic acid treatment on steel and blast furnace slags. Calcium-Looping conditions in this application involve carbonation at high temperature under high CO_2 concentration whereas calcination is carried out at relatively lower temperatures. Under these conditions, the main mechanism that limits the carbonation performance of CaO is pore plugging.

The raw slag samples do not present free $CaO/CaCO_3$ in their composition, which requires a simple acid pretreatment to obtain calcium acetate and calcium magnesium acetate that decompose to CaO upon calcination. The results obtained for the diverse steel and blast furnace slags analysed indicate that the multicycle conversion of the synthesized samples is kept at a high and stable value if the presence of Si is avoided by means of filtration applied as an intermediate step during the acetic acid treatment. Otherwise, porosity is enhanced after calcination which promotes pore plugging thus hindering the multicycle conversion at CaL conditions for CSP storage. The presence of Al in the blast furnace slags by a high amount has been also identified as a detrimental issue for the multicycle performance of the synthesized Ca based materials due to the irreversible formation of calcium aluminates upon calcination. These observations indicate that calcium and calcium magnesium acetates could be considered as good candidates to be used for thermochemical energy storage by means for the CaL process.

Acknowledgments

Financial support by the Spanish Government Agency Ministerio de Economia y Competitividad (contracts CTQ2014-52763-C2-2-R and CTQ2014-52763-C2-1-R) is acknowledged. AP thanks VPPI-US for this current contract. We gratefully thank the XRD, SEM and Functional Characterization Services of the Innovation, Technology and Research Centre of the University of Seville (CITIUS).

Bibliography

1. Framework Convention on Climate Change, U.N., *Conference of the Parties*. 30/11/2015-11/12-2015: Paris.
2. Lewis, N.S., *Research opportunities to advance solar energy utilization.* Science, 2016. **351**(6271).
3. Janz, G.J., et al., *Physical Properties Data Compilations Relevant to Energy Storage. II. Molten Salts: Data on Single and Multi-Components Salt Systems*. 1979.
4. Ortega-Fernández, I., et al., *Thermophysical characterization of a by-product from the steel industry to be used as a sustainable and low-cost thermal energy storage material.* Energy, 2015. **89**: p. 601-609.
5. Gimenez, P. and S. Fereres, *Effect of Heating Rates and Composition on the Thermal Decomposition of Nitrate Based Molten Salts.* Energy Procedia, 2015. **69**: p. 654-662.
6. Tzvetkoff, T. and J. Kolchakov, *Mechanism of growth, composition and structure of oxide films formed on ferrous alloys in molten salt electrolytes—a review.* Materials Chemistry and Physics, 2004. **87**(1): p. 201-211.
7. Bauer, T., et al., *Material aspects of Solar Salt for sensible heat storage.* Applied Energy, 2013. **111**: p. 1114-1119.
8. Paksoy, H.Ö., *Thermal Energy Storage for Sustainable Energy Consumption*. 2007.
9. Mahlia, T.M.I., et al., *A review of available methods and development on energy storage; Technology update.* Renewable and Sustainable Energy Reviews, 2014. **33**: p. 532-545.
10. Sakellariou, K.G., et al., *Calcium oxide based materials for thermochemical heat storage in concentrated solar power plants.* Solar Energy, 2015. **122**: p. 215-230.
11. Benitez-Guerrero, M., et al., *Large-scale high-temperature solar energy storage using natural minerals.* Solar Energy Materials and Solar Cells, 2017. **168**: p. 14-21.
12. Chacartegui, R., et al., *Thermochemical energy storage of concentrated solar power by integration of the calcium looping process and a CO2 power cycle.* Applied Energy, 2016. **173**: p. 589-605.
13. Alovisio, A., et al., *Optimizing the CSP-Calcium Looping integration for Thermochemical Energy Storage.* Energy Conversion and Management, 2017. **136**: p. 85-98.
14. Avila-Marin, A.L., *Volumetric receivers in Solar Thermal Power Plants with Central Receiver System technology: A review.* Solar Energy, 2011. **85**(5): p. 891-910.
15. Wang, Y., S. Lin, and Y. Suzuki, *Study of Limestone Calcination with CO2 Capture: Decomposition Behavior in a CO2 Atmosphere.* Energy & Fuels, 2007. **21**(6): p. 3317-3321.
16. Christen, G.L., M., *US3611676A*. 1971.
17. Valverde, J.M. and S. Medina, *Reduction of Calcination Temperature in the Calcium Looping Process for CO2 Capture by Using Helium: In Situ XRD Analysis.* ACS Sustainable Chemistry & Engineering, 2016. **4**(12): p. 7090-7097.
18. Sarrion, B., et al., *On the Multicycle Activity of Natural Limestone/Dolomite for Thermochemical Energy Storage of Concentrated Solar Power.* Energy Technology, 2016. **4**(8): p. 1013-1019.

19. Meier, A., et al., *Solar chemical reactor technology for industrial production of lime.* Solar Energy, 2006. **80**(10): p. 1355-1362.
20. Badie, J.M., et al., *52 Decarbonation of calcite and phosphate rock in solar chemical reactors.* Chemical Engineering Science, 1980. **35**(1): p. 413-420.
21. Meier, A., et al., *Design and experimental investigation of a horizontal rotary reactor for the solar thermal production of lime.* Energy, 2004. **29**(5): p. 811-821.
22. Meier, A., et al., *Multitube Rotary Kiln for the Industrial Solar Production of Lime.* Journal of Solar Energy Engineering, 2005. **127**(3): p. 386-395.
23. Imhof, A., *Decomposition of limestone in a solar reactor.* Renewable Energy, 1997. **10**(2): p. 239-246.
24. Blamey, J., et al., *The calcium looping cycle for large-scale CO2 capture.* Progress in Energy and Combustion Science, 2010. **36**(2): p. 260-279.
25. Valverde, J.M., *Ca-based synthetic materials with enhanced CO2 capture efficiency.* Journal of Materials Chemistry A, 2013. **1**(3): p. 447-468.
26. Perejón, A.R., Luis M.; Lara, Yolanda; Lisbona, Pilar; Martínez, Ana; Valverde, Jose Manuel, *The Calcium-Looping technology for CO2 capture: On the important roles of energy integration and sorbent behavior.* On the review, 2015.
27. Valverde, J.M., P.E. Sanchez-Jimenez, and L.A. Perez-Maqueda, *Role of precalcination and regeneration conditions on postcombustion CO2 capture in the Ca-looping technology.* Applied Energy, 2014. **136**: p. 347-356.
28. Hu, Y., et al., *Investigation of novel naturally occurring manganocalcite for CO2 capture under oxy-fuel calcination.* Chemical Engineering Journal, 2016. **296**: p. 412-419.
29. Manovic, V. and E.J. Anthony, *Thermal Activation of CaO-Based Sorbent and Self-Reactivation during CO2 Capture Looping Cycles.* Environmental Science & Technology, 2008. **42**(11): p. 4170-4174.
30. *Position Paper on the Status of Ferrous Slag. Waste Framework Directive*, in *Regulation*. 2012.
31. Philibert, C., *Technology roadmap: concentrating solar power*. 2010: OECD/IEA.
32. Quader, M.A., et al., *A comprehensive review on energy efficient CO2 breakthrough technologies for sustainable green iron and steel manufacturing.* Renewable and Sustainable Energy Reviews, 2015. **50**: p. 594-614.
33. Liu, J., et al., *Thermal energy recovery from high-temperature blast furnace slag particles.* International Communications in Heat and Mass Transfer, 2015. **69**: p. 23-28.
34. Xiong, B., et al., *Modeling and performance analysis of a two-stage thermoelectric energy harvesting system from blast furnace slag water waste heat.* Energy, 2014. **77**: p. 562-569.
35. Oss, H.G.v., *Iron and Steel Slag.* U.S. Geological Survey, Mineral Commodity Summaries, 2015.
36. Miranda-Pizarro, J., et al., *Use of steel slag for CO2 capture under realistic calcium-looping conditions.* RSC Advances, 2016. **6**(44): p. 37656-37663.
37. Lee, S., et al., *CO2 sequestration technology through mineral carbonation: An extraction and carbonation of blast slag.* Journal of CO2 Utilization, 2016. **16**: p. 336-345.
38. Teir, S., et al., *Case study for production of calcium carbonate from carbon dioxide in flue gases and steelmaking slag.* Journal of CO2 Utilization, 2016. **14**: p. 37-46.

39. Hu, Y., et al., *Structurally improved CaO-based sorbent by organic acids for high temperature CO2 capture.* Fuel, 2016. **167**: p. 17-24.
40. Ridha, F.N., et al., *Assessment of limestone treatment with organic acids for CO2 capture in Ca-looping cycles.* Fuel Processing Technology, 2013. **116**: p. 284-291.
41. Koga, N. and J.M. Criado, *The influence of mass transfer phenomena on the kinetic analysis for the thermal decomposition of calcium carbonate by constant rate thermal analysis (CRTA) under vacuum.* International Journal of Chemical Kinetics, 1998. **30**(10): p. 737-744.
42. Li, Y.J., et al., *CO2 capture efficiency and energy requirement analysis of power plant using modified calcium-based sorbent looping cycle.* Energy, 2011. **36**(3): p. 1590-1598.
43. Li, Y.J., et al., *Cyclic calcination/carbonation looping of dolomite modified with acetic acid for CO2 capture.* Fuel Processing Technology, 2008. **89**(12): p. 1461-1469.
44. Judd, M.D., B.A. Plunkett, and M.I. Pope, *Thermal-decomposition of calcium, sodium, silver and copper(ii) acetates.* Journal of Thermal Analysis, 1974. **6**(5): p. 555-563.
45. Niu, S.L., et al., *Thermogravimetric analysis of the relationship among calcium magnesium acetate, calcium acetate and magnesium acetate.* Applied Energy, 2010. **87**(7): p. 2237-2242.
46. Han, D.H. and H.Y. Sohn, *Calcined calcium magnesium acetate as a superior SO2 sorbent: I. Thermal decomposition.* Aiche Journal, 2002. **48**(12): p. 2971-2977.
47. Silaban, A., M. Narcida, and D.P. Harrison, *Calcium Magnesium Acetate: An emerging bulk chemical for environmental applications Calcium acetate as a sorbent precursor for the removal of carbon dioxide from gas streams at high temperature.* Resources, Conservation and Recycling, 1992. **7**(1): p. 139-153.
48. Musumeci, A.W., R.L. Frost, and E.R. Waclawik, *A spectroscopic study of the mineral paceite (calcium acetate).* Spectrochimica Acta Part A: Molecular and Biomolecular Spectroscopy, 2007. **67**(3–4): p. 649-661.
49. Adanez, J., L.F. de Diego, and F. Garcia-Labiano, *Calcination of calcium acetate and calcium magnesium acetate: effect of the reacting atmosphere.* Fuel, 1999. **78**(5): p. 583-592.
50. Dionysiou, D., M. Tsianou, and G. Botsaris, *Extractive Crystallization for the Production of Calcium Acetate and Magnesium Acetate from Carbonate Sources.* Industrial & Engineering Chemistry Research, 2000. **39**(11): p. 4192-4202.
51. Stendardo, S., L.K. Andersen, and C. Herce, *Self-activation and effect of regeneration conditions in CO2–carbonate looping with CaO–Ca12Al14O33 sorbent.* Chemical Engineering Journal, 2013. **220**: p. 383-394.
52. Valverde, J.M., A. Perejon, and L.A. Perez-Maqueda, *Enhancement of Fast CO2 Capture by a Nano-SiO2/CaO Composite at Ca-Looping Conditions.* Environmental Science & Technology, 2012. **46**(11): p. 6401-6408.
53. Valverde, J.M., P.E. Sanchez-Jimenez, and L.A. Perez-Maqueda, *Effect of Heat Pretreatment/Recarbonation in the Ca-Looping Process at Realistic Calcination Conditions.* Energy & Fuels, 2014. **28**(6): p. 4062-4067.
54. Sanchez-Jimenez, P.E., L.A. Perez-Maqueda, and J.M. Valverde, *Nanosilica supported CaO: A regenerable and mechanically hard CO2 sorbent at Ca-looping conditions.* Applied Energy, 2014. **118**: p. 92-99.

55. Lu, H., E.P. Reddy, and P.G. Smirniotis, *Calcium Oxide Based Sorbents for Capture of Carbon Dioxide at High Temperatures.* Industrial & Engineering Chemistry Research, 2006. **45**(11): p. 3944-3949.
56. Pinheiro, C.I.C., et al., *Waste Marble Powders as Promising Inexpensive Natural CaO-Based Sorbents for Post-Combustion CO2 Capture.* Industrial & Engineering Chemistry Research, 2016. **55**(29): p. 7860-7872.
57. Valverde, J.M., et al., *Role of crystal structure on CO2 capture by limestone derived CaO subjected to carbonation/recarbonation/calcination cycles at Ca-looping conditions.* Applied Energy, 2014. **125**: p. 264-275.
58. Valverde, J.M. and S. Medina, *Crystallographic transformation of limestone during calcination under CO2.* Physical Chemistry Chemical Physics, 2015. **17**(34): p. 21912-21926.